Accurate Retrieval of Target Structures and Laser Parameters of Few-Cycle Pulses from Photoelectron Momentum Spectra

S. Micheau,[1] Zhangjin Chen,[1] A. T. Le,[1] J. Rauschenberger,[2] M. F. Kling,[2] and C. D. Lin[1]

[1]*Department of Physics, Kansas State University, Manhattan, Kansas 66506, USA*
[2]*Max-Planck Institute of Quantum Optics, Hans-Kopfermann-Straße 1, 85748 Garching, Germany*
(Received 22 August 2008; published 18 February 2009)

We illustrate a new method of analyzing three-dimensional momentum images of high-energy photo-electrons generated by intense phase-stabilized few-cycle laser pulses. Using photoelectron momentum spectra that were obtained by velocity-map imaging of above-threshold ionization of xenon and argon targets, we show that the absolute carrier-envelope phase, the laser peak intensity, and pulse duration can be accurately determined simultaneously (with an error of a few percent). We also show that the target structure, in the form of electron-target ion elastic differential cross sections, can be retrieved over a range of energies. The latter offers the promise of using laser-generated electron spectra for probing dynamic changes in molecular targets with subfemtosecond resolution.

Developments in laser technology make it possible to produce intense laser pulses that contain only a few cycles [1]. For these few-cycle pulses, the time dependence of the electric field of a linearly polarized laser can be written as $E(t) = E_0(t)\cos(\omega t + \varphi)$, where $E_0(t)$ is the pulse envelope, ω the carrier frequency, and φ the carrier-envelope phase (CEP). By changing the CEP, an additional new control knob becomes available to experimentalists for manipulating laser-matter interactions [2,3]. To stabilize the CEP, present methods use a locking mechanism which measures only the change of the CEP and is thus blind to its absolute value.

A number of methods have been proposed or used to measure the absolute phase [4–7]. Current phase retrieval methods are based either on measuring the number of above-threshold ionization (ATI) photoelectrons ejected by atoms [7] or on the generated high-order harmonics spectra [5]. In this Letter, we analyze the CEP-dependent high-energy electron momentum spectra such as those reported in Kling *et al.* [8]. While different values of the CEP are known to result in a left-right asymmetry between the number of electrons detected on the "left" and "right" sides along the polarization axis, the determination of the absolute CEP relies on a comparison with simulations obtained from solving the time-dependent Schrödinger equation (TDSE). Here we demonstrate an alternative robust approach based on the recently developed quantitative rescattering (QRS) theory [9–11] for high-energy ATI (HATI) electrons. We reanalyze the data reported in Kling *et al.* [8] and show that the absolute CEP, the pulse duration, and the peak intensity of the few-cycle pulses can be determined accurately. Furthermore, elastic differential cross sections (DCS's) between target ions and *free* electrons [12,13] can also be extracted from the data.

The experiment was explained in detail earlier [8]. Briefly, linear polarized phase-stable few-cycle pulses at a central wavelength of 760 nm were focused into the center of the electron optics of a velocity-map imaging apparatus. Here, we obtained left and right photoelectron spectra by angular integration of the momentum images over 10° along the two sides of the laser polarization axis. Spectra collected without phase stabilization have been used to correct for inhomogeneities in the detector response.

To understand HATI spectra, we rely on the rescattering concept in strong field ionization which has been around for nearly two decades [14,15]. According to this model, electrons which are released earlier by tunneling ionization may be driven back to revisit the parent ion when the direction of the laser's electric field changes. From the earlier work of DiMauro and coworkers [16,17] and of Paulus *et al.* [18,19], it has been shown that the HATI photo-electrons are generated via large-angle elastic backscattering of these returning electrons by the parent ion. The recently developed QRS model [10,11] puts this qualitative rescattering concept on the quantitative level, by showing that HATI momentum spectra $I(p, \theta)$ can be expressed as

$$I(p, \theta) = W(p_r)\sigma(p_r, \theta_r). \tag{1}$$

Here $\sigma(p_r, \theta_r)$ is the elastic scattering DCS between the target ion and *free* electrons, i.e., without the presence of laser, and the proportional constant $W(p_r)$ is interpreted as the returning electron wave packet. [We emphasize that Eq. (1) was first derived in [9] for a single value of p_r only. In [10] it was extended to the whole rescattering region, and the new model is called the QRS model.] The relation between the HATI electron momentum **p** at the end of the laser pulse and the momentum $\mathbf{p}_r$ of the returning electron right after its elastic collision with the target ion is given by $\mathbf{p} = -\mathbf{A}_r + \mathbf{p}_r$, with the magnitudes $A_r = p_r/1.26$. The additional $-\mathbf{A}_r$ term accounts for the velocity gained by the electron from the time of elastic collision till the end of the laser pulse. Here $\mathbf{A}_r$ is the vector potential at the time of recollision, and the electron scattering angle θ_r is measured from the "incident" direction of the returning elec-

tron toward the target ion. Atomic units are used in this Letter unless otherwise noted. The relation $\mathbf{p} = -\mathbf{A}_r + \mathbf{p}_r$ shows that high-energy photoelectrons are generated only when the returning electrons are backscattered, i.e., for $\theta_r > 90°$.

The factorization in Eq. (1) has been tested previously [10] for HATI electrons. By treating the atomic target as an active electron in a model potential, $I(p, \theta)$ can be accurately calculated by solving the TDSE [20], and the DCS can be calculated easily from the potential scattering theory described in standard quantum mechanics textbooks. The validity of Eq. (1) is confirmed by showing that the ratio $I(p, \theta)/\sigma(p_r, \theta_r)$ is independent of the angle θ_r. We call the ratio the returning electron wave packet $W(p_r)$. Alternatively, one can also calculate $I(p, \theta)$ approximately using the so-called 2nd-order strong field approximation (SFA2) [21]. In SFA2, electron-ion interaction is treated to first order only; thus the DCS, $\sigma(p_r, \theta_r)$, is calculated by the first Born approximation. By taking the ratio as before using Eq. (1), one can also obtain a $W(p_r)$. In [21] it has been shown that the wave packets $W(p_r)$ obtained from SFA2 and from TDSE have the same shape. They differ by a normalization factor, reflecting the fact that the tunneling ionization rate calculated using SFA is different from solving the TDSE. Thus in the QRS theory, we obtain HATI electron spectra by multiplying $W(p_r)$ from SFA2 with the accurate DCS from electron-ion collisions. The resulting HATI spectra thus obtained have comparable accuracy as from solving the TDSE [10]. Using the QRS theory, we reduce the computation time by a factor of about 1000 compared to solving TDSE. More importantly, using QRS, we can examine how the returning electron wave packet depends on the laser parameters, as shown below.

In Fig. 1(a) we depict a five-cycle, 760 nm laser pulse with peak intensity of 1.0×10^{14} W/cm^2 for $\varphi = 0$, showing both the electric field and vector potential. The wave packets calculated from the Xe target are shown in Fig. 1(b). For the left wave packet, most of the electrons are ionized at L_1 and return at A_1 [Fig. 1(a)]. The wave packet oscillates due to interference with electrons ionized at L_2 and returned at A_2. Similarly, a right wave packet can be derived from electrons that are ionized at R_1 and R_2. The R_1 peak in Fig. 1(b) shows no interference since electrons ionized at R_2 return with low energies. Clearly, features of the wave packet resulting from each half cycle can be identified. Note that the ionization yield depends on the value of the peak electric field when the electrons are ionized, while the peak momentum of the returning electrons depends on the value of the vector potential when the electron returns. By changing the CEP, the peak electric field and vector potential evolve smoothly; thus the wave packets evolve smoothly with CEP as well [see Figs. 1(c) and 1(d)].

Since the electron wave packets derived above cannot be measured directly, we examined how the HATI electron spectra evolve with the change of CEP. We used the QRS model to calculate the HATI electron momentum spectra
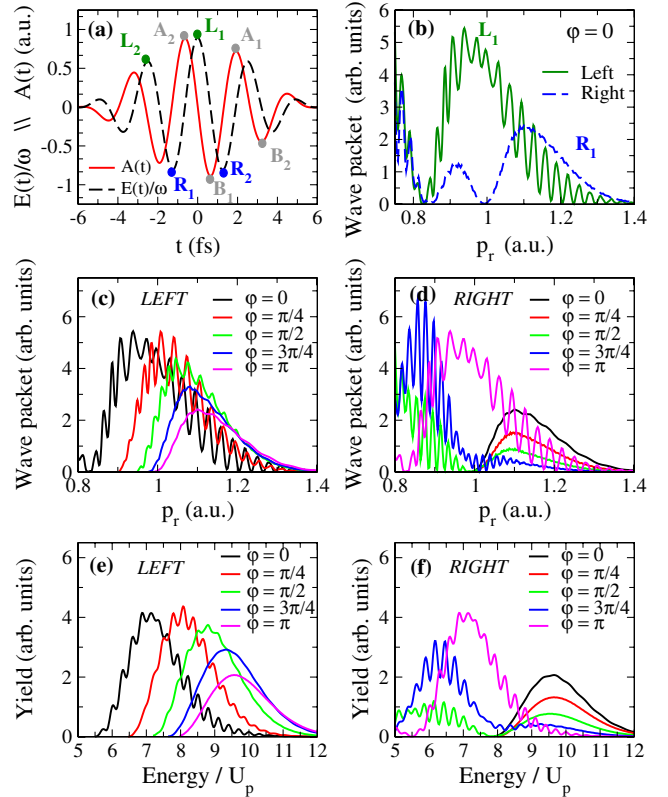

FIG. 1 (color online).   (a) Electric field and vector potential of a 760 nm five-cycle laser pulse at 1×10^{14} W/cm^2 for CEP $\varphi = 0$. (b) Left and right wave packets calculated for the laser pulse in (a) for xenon. (c, d) The evolution of left and right wave packets with CEP, respectively. (e, f) Theoretical left and right high-energy photoelectron energy spectra calculated by the QRS model vs CEP. The spectra have been obtained by angular integration over a cone of 10° along the laser polarization axis.

$I(p, \theta)$ of Xe using the wave packets shown in Figs. 1(c) and 1(d). By integrating $I(p, \theta)$ for θ within 10° from the polarization axis, we show in Fig. 1(e) and 1(f) the electron energy spectra vs the CEP. Compared to Figs. 1(c) and 1(d), the peaks of the electron spectra mimic the peaks in the wave packets nicely.

The theoretical spectra in Figs. 1(e) and 1(f) still cannot be compared to experiments. For a tightly focused laser, the intensity within the interaction volume is not uniform. Thus the theoretical spectra have to account for the intensity distribution within the interaction region. By assuming the spatial intensity distribution of a Gaussian beam, we show in Figs. 2(a) and 2(b) the volume-integrated theoretical left and right electron spectra for a peak intensity of 1.1×10^{14} W/cm^2 and pulse duration of 6.7 fs. The peak intensity (at the laser focus) and the pulse duration are the results from best fitting to the experimental data [8] (see below). In Fig. 2(c) and 2(d) we show the electron spectra from the experimental data [8]. By comparing the curves of the same colors along each column, we can see that there is a good agreement between the simulation and the experimental spectra on the left and on the right, respectively. For

the small discrepancy for each CEP it is understood that the CEP's in the experiment are not exactly at 0, $\pi/4, \ldots, \pi$, as listed in the theory since only discrete values of CEP are measured experimentally.

In Fig. 3(a), the peak energy vs CEP from the experimental data, as shown in Fig. 2(c), is shown in red crosses. By varying the peak intensity as well as the pulse duration, from the best fit to the experimental data we obtained the experimental peak intensity of 1.1×10^{14} W/cm^2 and pulse duration of 6.7 fs. By changing the peak intensity, the absolute energy values of the peak position become incorrect; see the green X's in the figure where peak intensities of 1.0 and 1.2×10^{14} W/cm^2, respectively, were used for the same pulse duration of 6.7 fs. For a given intensity, change of pulse duration results in a change of slope of the peak position vs CEP. This is shown for two examples (green circles and black triangles) with pulse durations of 6.0 fs and 7.0 fs, respectively, in the figure. It is clear that the slope becomes flatter as the pulse duration is increased.

The above analysis was based on spectra obtained by integrating an angular range of 10° along the polarization axis. If other angles are used, the peak positions and the slope would be slightly different, both experimentally and theoretically. We have checked that the retrieved peak intensity, pulse length, and absolute CEP do not depend on the range of angular integration. For a large angular range of integration the structure in the HATI spectra would lose contrast. We found that 40° is the reasonable upper limit. In Fig. 3(a), we only examined the CEP dependence of the left wave packets. For CEP near π, the curve begins to flatten out; i.e., the peak positions no longer change significantly with increase of CEP. In this case, we can examine peak positions of the right-side spectra. For example, the peak positions for CEP of $3\pi/4$ and π curves do not change significantly in Fig. 2(c), but their changes are quite large in Fig. 2(d). By examining the left and right electron spectra separately, we can check the self-consistency of the data retrieved. Such "luxury" is not available if one used the left-right asymmetry analysis [7,8]. Unlike the present method, as illustrated in Fig. 3(a), where the influence of peak intensity, pulse duration, and the CEP plays different roles, using the left-right asymmetry, their influence on the asymmetry parameters cannot be separated; thus the method is less accurate. In fact, we found major discrepancies with the values of the CEP obtained in [8].

We also analyzed the data from Ar in the same manner. According to the QRS theory, if the laser parameters are identical, the returning wave packet should be identical (independent of the target) except for an overall normalization (due to the different tunneling rates). Using the data from Kling *et al.* [8] we found that best agreement is achieved for a pulse duration of 6.7 fs and peak intensity of 1.0×10^{14} W/cm^2 [see Fig. 3(b)]. Compared to the data retrieved from Xe, the peak intensity is 10% smaller. Experimentally this small intensity difference between the two data sets is considered to be likely.

After extracting the laser parameters, we next consider structural information from the HATI electron momentum spectra. According to Eq. (1), the DCS, $\sigma(p_r, \theta_r)$, for a fixed incident electron momentum p_r can be obtained from the measured $I(p, \theta)$ [9,10], and the extracted DCS should be independent of the lasers—in this case, independent of the CEP. Unlike the theory presented in [9] where DCS is extracted only from electrons returning with maximum kinetic energy of $3.17U_p$, in the experimental data, electrons are collected from different regions within the focal volume where U_p varies from one point to another. Thus the success of [12,13] in retrieving accurate DCS's is
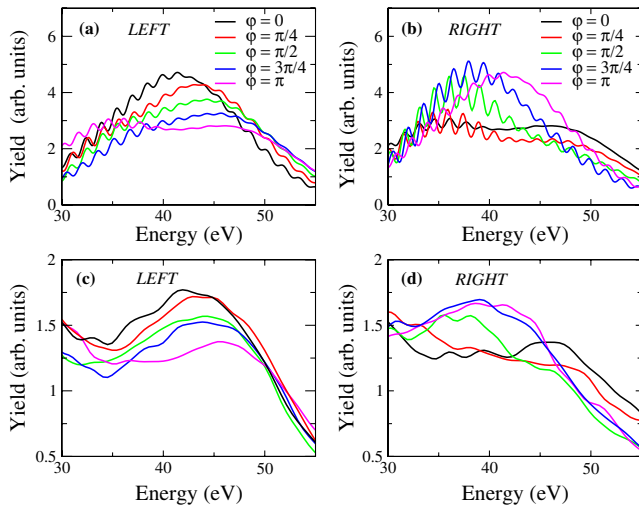

FIG. 2 (color online).   (a, b) Volume-integrated left and right high-energy Xe photoelectron spectra from the QRS model for a laser pulse at 760 nm, pulse duration of 6.7 fs, and peak intensity of 1.1×10^{14} W/cm^2 and different CEP. The peak intensity and pulse duration are obtained from the best fit to the experimental data of Kling *et al.* [8], shown in (c) and (d) for left and right electron spectra, respectively. All data are from integrating over 10° along the polarization axis. The remaining small discrepancy is partly because the CEP values in the experimental data are not at exactly the same values as in the theory (see text).
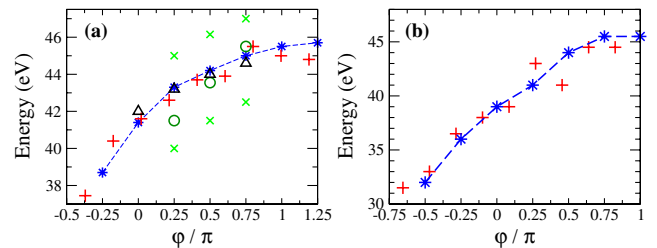

FIG. 3 (color online).   (a) Peak energies vs the CEP from the electron spectra on the left for a Xe target. Red crosses represent experimental data shown in Fig. 2(c); blue asterisks connected by a line represent best theoretical fits; other symbols show how the peak energies change when peak intensity or pulse duration are varied from the best fit (see text). (b) Similar analysis using an Ar target.
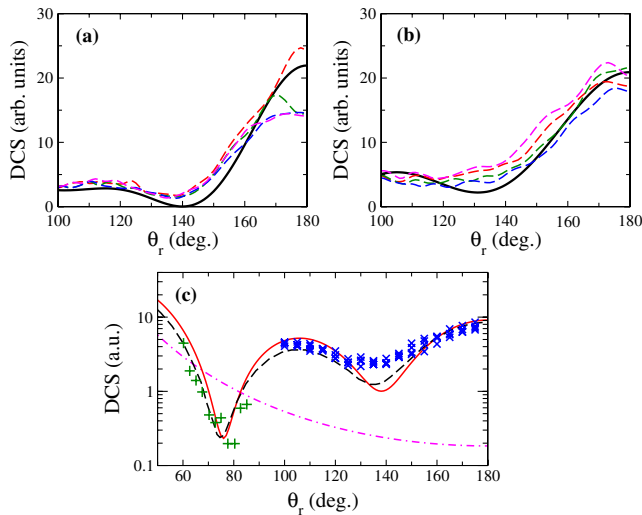
FIG. 4 (color online). (a) Differential elastic scattering cross sections for Xe^+ ions by free electrons with incident momentum of $p_r = 1.2$ a.u.. Solid line: theoretical result calculated from a model potential for Xe. Dashed lines: DCS's extracted from experimental data of [8] with different CEP's. (b) Similar to (a) except for Ar, for $p_r = 0.9$ a.u.. (c) Elastic scattering DCS's of Ar^+ ion by free electrons with $p_r = 1.1$ a.u. over a large angular range. The lines are from three different theoretical calculations (see text). The symbols are from an electron-Ar^+ collision experiment [22] for small angles and from the present HATI spectra for large angles. The theoretical curves do not include experimental angular resolutions.

implicitly based on the QRS model, not the theory in [9]. Here we further demonstrate this procedure using the experimental data from [8]. In Fig. 4(a), the DCS's for Xe at $p_r = 1.2$ a.u. extracted from experimental data of different CEP's are shown. In Fig. 4(b), the same from Ar at $p_r = 0.9$ a.u. are shown. Indeed the DCS's extracted from different CEP data are very close to each other, and they are in good agreement with the theoretical DCS's calculated from the single active electron approximation. The discrepancy is partly due to the angular resolution in the experiment, but the neglect of many-electron effects in treating Xe as a one-electron atom may also contribute. In Fig. 4(c) we further show the DCS extracted from the HATI spectra for $p_r = 1.1$ a.u.. This can be compared to experimental results obtained from standard electron collisions with Ar^+ ions measured by Brotton *et al.* [22] at 16 eV. This figure also includes theoretical results using our one-electron model potential [9] (dashed line) and calculations which treated Ar^+ as a many-electron system at the Hartree-Fock level [22] (solid line). The two theories agree reasonably well, both showing two DCS minima. On the other hand, Coulomb scattering alone would give a monotonic angular distribution (dash-dotted line), in disagreement with experiments. Experimentally, the electron collision data cover the smaller angular region, including

the first minimum, while the DCS's deduced from the HATI spectra cover the large-angle region, including the second minimum. Both experimental data are normalized to the theory to obtain optimum agreement. This figure illustrates that one can obtain accurate relative DCS's from laser-generated HATI spectra.

In summary, using the quantitative rescattering theory we have demonstrated a very efficient and accurate method for determining simultaneously the absolute carrier-envelope phase, peak intensity, and pulse duration of few-cycle laser pulses by analyzing the experimental high-energy ATI electron momentum spectra. At the same time, the theory also shows that the structure of the target, in the form of elastic electron-target ion scattering cross sections, can be accurately extracted even if the laser parameters are not accurately known. Extending such measurements to molecular targets, it shows that laser parameters, as well as the nature of the target, can all be accurately retrieved at the same time, thus opening up great opportunities of using few-cycle laser pulses for studying time-resolved chemical structural changes with subfemto-second resolution.

[1] A. Baltuška *et al.*, Nature (London) **421,** 611 (2003).
[2] M. F. Kling *et al.*, Science **312,** 246 (2006).
[3] G. G. Paulus *et al.*, Nature (London) **414,** 182 (2001).
[4] A. Apolonski *et al.*, Phys. Rev. Lett. **92,** 073902 (2004).
[5] C. A. Haworth *et al.*, Nature Phys. **3,** 52 (2007).
[6] M. Kreß *et al.*, Nature Phys. **2,** 327 (2006).
[7] G. G. Paulus *et al.*, Phys. Rev. Lett. **91,** 253004 (2003).
[8] M. F. Kling *et al.*, New J. Phys. **10,** 025 024 (2008).
[9] T. Morishita *et al.*, Phys. Rev. Lett. **100,** 013903 (2008).
[10] Z. Chen *et al.*, arXiv:0804.3669.
[11] A. T. Le, T. Morishita, and C. D. Lin, Phys. Rev. A **78,** 023814 (2008).
[12] M. Okunishi *et al.*, Phys. Rev. Lett. **100,** 143001 (2008).
[13] D. Ray *et al.*, Phys. Rev. Lett. **100,** 143002 (2008).
[14] P. B. Corkum, Phys. Rev. Lett. **71,** 1994 (1993).
[15] K. Schafer *et al.*, Phys. Rev. Lett. **70,** 1599 (1993).
[16] B. Walker *et al.*, Phys. Rev. Lett. **77,** 5031 (1996).
[17] B. Yang *et al.*, Phys. Rev. Lett. **71,** 3770 (1993).
[18] G. G. Paulus *et al.*, Phys. Rev. Lett. **72,** 2851 (1994).
[19] G. G. Paulus *et al.*, J. Phys. B **27,** L703 (1994).
[20] T. Morishita *et al.*, Phys. Rev. A **75,** 023407 (2007).
[21] Z. Chen *et al.*, Phys. Rev. A **76,** 043402 (2007).
[22] S. J. Brotton *et al.*, Phys. Rev. A **66,** 062706 (2002).